Turkish Journal of Electrical Engineering & Computer Sciences

http://journals.tubitak.gov.tr/elektrik/

Research Article

Turk J Elec Eng & Comp Sci
(2016) 24: 961 – 972
© TÜBİTAK
doi:10.3906/elk-1312-104

# Modeling and control of a doubly fed induction generator with a disturbance observer: a stator voltage oriented approach

**Eşref Emre ÖZSOY[1,*], Edin GOLUBOVIC[2], Asıf SABANOVIC[2], Seta BOGOSYAN[1], Metin GÖKAŞAN[1]**

[1]Faculty of Engineering, İstanbul Technical University, İstanbul, Turkey

[2]Faculty of Engineering and Natural Sciences, Sabancı University, İstanbul, Turkey

**Received:** 14.12.2013 • **Accepted/Published Online:** 23.01.2014 • **Final Version:** 23.03.2016

**Abstract:** The popularity of renewable energy conversion systems, and especially of wind energy, has been growing in recent years. Doubly fed induction generator (DFIG)-based wind energy systems are extensively used due to their wide range of active and reactive power controllability. Conventional DFIG control structures consist of decoupled PI rotor current controllers with stator flux orientation and machine parameter-dependent compensating terms. The accuracy of stator flux calculations is dependent on how accurately the stator resistance is known. Integration problems also exist and additional low-pass filters are implemented to accurately calculate the stator flux. In the current study, machine-dependent compensating terms are estimated with a first-order low-pass filter disturbance observer. Therefore, a single proportional (P) controller is sufficient to control decoupled rotor currents. The proposed controller structure is implemented on a MATLAB/Simulink platform with the parameters of 500 kW DFIG used in the MİLRES (Turkish National Wind Energy) project. The proposed controller is also experimentally validated in an experimental setup.

**Key words:** Doubly fed induction generator, disturbance observer, wind energy

## 1. Introduction

Research on renewable energy conversion systems is of great importance due to the rapid consumption of fuel resources and environmental issues. Wind energy conversion systems appear to be the fastest growing technology and most of the electrical energy generated by renewable sources is from wind energy conversion systems [1]. Doubly fed induction generator (DFIG)-based wind turbines have important advantages as compared with other wind energy conversion systems. For example, 30% of rated stator power is sufficient for the rotor side inverter circuit to achieve 4-quadrant stator active and reactive power flow with a speed variation of around $\pm 25\%$. This reduces the cost and complexity of the overall system.

Considerable research studies are encountered about DFIG modeling and control in the literature. DFIG dynamic equations are fully written in [1,2]. A complete simulation and the modeling for high-power DFIG wind farms are given in [3]. A reduced-order DFIG dynamic model was also proposed in this study due to simulation constraints.

From an orientation-frame point of view, stator flux [4] and stator voltage orientation [5] can be encountered in which the position of the stator flux or voltage space vector is aligned with the d axis of the d-q frame. Stator flux orientation control techniques are dependent on the accuracy of stator resistance information.

*Correspondence: eozsoy@itu.edu.tr

Integration problems also exist and additional low-pass filters are implemented to accurately calculate stator flux [4]. The effect of the stator resistance value can be neglected in flux calculations and the stator voltage orientation could be applied by adding a 90° phase shift to the voltage angle. This may cause an additional coupling effect in active and reactive power control, which can be compensated by implementing additional controllers in the outer loop as given in [5]. It was claimed in [6] that the controller performances of both orientation frames are equivalent.

The idea of a stator voltage orientation with a disturbance observer started with [7]. The scheme of [7] consists of simulation results of a direct stator active and reactive power control with a disturbance observer.

Synchronization is another issue to smoothly connect a DFIG to the grid. Grid and generated stator voltages must be collinear, which means equal in phase and amplitude, before the DFIG is connected to the grid to prevent high currents. The majority of contributions focus on a mode of operation in which the DFIG is already connected to the grid. The synchronization procedure was comprehensively analyzed in [8] with important citations.

There are also many studies examining different control perspectives. Direct power control strategies that directly control stator power without rotor current control loops were reported in [9,10]. Sliding mode controller structures [11,12] are also important contributions that deal with energy maximization and robustness against disturbances. There are also reputable studies that considered robustness against grid voltage problems [13–15].

The current study focuses on designing a novel robust stator voltage oriented DFIG controller structure with a low-pass filter first-order disturbance observer. The main contribution of this paper is to achieve a simpler controller as compared to the basic conventional schemes given in [4,5]. Machine-dependent compensating terms are accurately estimated with the first-order low-pass filter disturbance observer. This prevents the necessity of accurately knowing the machine parameters, which may deteriorate according to physical conditions. Decoupled proportional rotor current controllers are sufficient to separately control stator active and reactive power. The parameters of the actual 500 kW DFIG in the MİLRES (Turkish National Wind Energy Systems) project are used for the MATLAB/Simulink-based system model. The proposed current controller is also implemented on a 1.1 kW DFIG experimental test bed.

The rest of the paper is organized as follows: the dynamic equations of the DFIG are given in Section 2; Section 3 provides a controller structure based on a first-order disturbance observer; simulation results of the proposed control structure are demonstrated in Section 4; experimental results are presented in Section 5; and the conclusions are summarized in Section 6.

## 2. DFIG dynamic equations

Before writing the dynamic equations, the $L_r$ value could be written as follows:

$$L_r = L_{rb} + \Delta L_r. \tag{1}$$

$L_{rb}$ is the inductance value at fundamental frequency. $\Delta L_r$ is the value that is affected by frequency and other physical disturbances. The DFIG dynamic equations in [1,2] can be rewritten as follows:

$$V_s = L_s \frac{dI_s}{dt} + R_s I_s + L_m \frac{dI_r}{dt} + M_s(I_s + M_r I_r), \tag{2}$$

$$V_r = L_{rb} \frac{dI_r}{dt} + \Delta L_r \frac{dI_r}{dt} + R_r I_r + L_m \frac{dI_s}{dt} + N_s(I_r + N_r I_s). \tag{3}$$

The matrices V, I, M, and N are defined as follows.

$$V = \begin{bmatrix} v_d & v_q \end{bmatrix}^T \quad I = \begin{bmatrix} i_d & i_q \end{bmatrix}^T \tag{4}$$

$$M_s = \begin{bmatrix} 0 & L_s\omega_s \\ -L_s\omega_s & 0 \end{bmatrix}, \quad M_r = \begin{bmatrix} 0 & \frac{L_m}{L_s} \\ -\frac{L_m}{L_s} & 0 \end{bmatrix} \tag{5}$$

$$N_s = \begin{bmatrix} 0 & L_s\omega_s \\ -L_s\omega_s & 0 \end{bmatrix}, \quad N_r = \begin{bmatrix} 0 & \frac{L_m}{L_r} \\ -\frac{L_m}{L_r} & 0 \end{bmatrix} \tag{6}$$

All rotor variables are referred to the stator side. The electromagnetic torque can be given as:

$$T_{em} = \frac{3}{2} pL_m(i_{rd}i_{sq} - i_{rq}i_{sd}). \tag{7}$$

Stator active and reactive power equations can be written as:

$$P_s = \frac{3}{2}(v_{sd}i_{sd} + v_{sq}i_{sq}), \tag{8}$$

$$Q_s = \frac{3}{2}(v_{sq}v_{sd} - v_{sd}i_{sq}) \tag{9}$$

The equation of motion can be given as:

$$\frac{d\omega_m}{dt} = \frac{1}{J}(T_m - T_e + b.\omega_m). \tag{10}$$

## 3. Control system

### 3.1. Stator voltage angle calculation

Rotating frames could be aligned differently according to the literature. The stator voltage angle is aligned with the d axis, with $v_s = v_{sd}$ and $v_{sq} = 0$. The voltage vectors and reference frames are given in Figure 1.

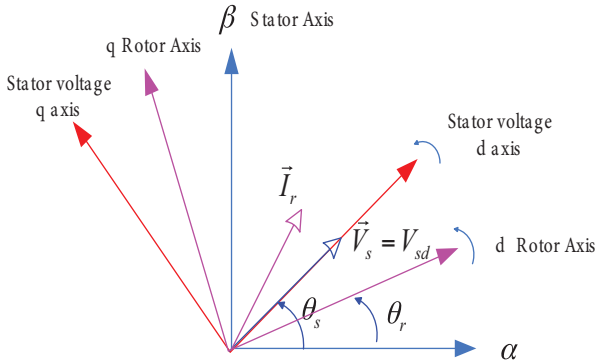


**Figure 1.** Voltage vectors and reference frames.

The voltage angle could be calculated by using the following formula:

$$\theta_s = \arctan\left(\frac{v_{s\beta}}{v_{s\alpha}}\right). \tag{11}$$

However, phase-locked loop (PLL) techniques that are more robust against voltage disturbances are widely used for phase and frequency detection of the voltage signal. Different PLL techniques can be encountered in the literature [16]. A basic PLL algorithm, given in Figure 2, is used in the simulations and experiments of the current study. Grid voltages, transformed into a dq coordinate system, are the inputs of the algorithm. The Q component of the voltage could be forced to zero with a PI controller. The output of the PI controller is the grid frequency. The integration of the grid frequency is the position of the signal. This position is used in the abc-dq calculation.

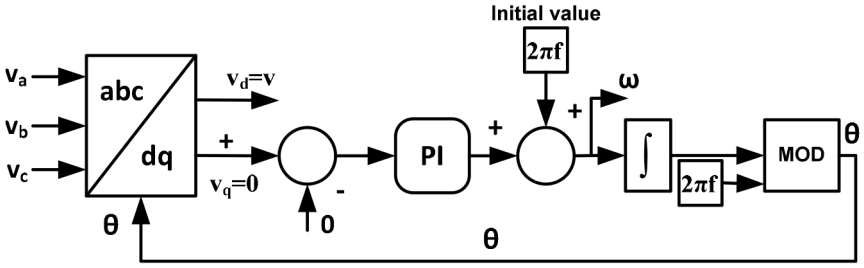


**Figure 2.** PLL algorithm.

### 3.2. Design of current controllers

The DFIG rotor voltage equation (Eq. (3)) must be rewritten for a simpler design of proportional rotor current controllers. All currents and voltages could be measured in real applications without any problems. However, machine parameters may deteriorate according to physical conditions. The aim of rewriting the equations is to separate the machine-dependent and machine-independent terms. Therefore, a simpler controller structure could be achieved. Rotor dynamics in Eq. (3) could be rewritten as follows:

$$\frac{dI_r}{dt}=\frac{V_r}{L_{rb}}+\underbrace{\left(-\frac{R_r}{L_r}V_r-\frac{L_m}{L_r}\frac{dI_s}{dt}+N_s(I_sN_rI_r)-\Delta L_r\frac{dI_r}{dt}\right)}_{V_r^{dis}}. \tag{12}$$

The vector $V_r^{dis}$ is defined as $V_r^{dis}=\begin{bmatrix} v_{rd}^{dis} & v_{rq}^{dis} \end{bmatrix}$; these are considered parameter-dependent disturbance terms. Eq. (12) could be simplified as follows:

$$\frac{dI_r}{dt}=\frac{V_r}{L_{rb}}+V_r^{dis}. \tag{13}$$

The derivative of errors for rotor currents can be written as:

$$\frac{d\varepsilon_r}{dt}=\frac{dI_r^{ref}}{dt}-\frac{dI_r}{dt}, \tag{14}$$

where $\varepsilon_{rd}=\begin{bmatrix} \varepsilon_{rd} & \varepsilon_{rq} \end{bmatrix}^T$.

Eqs. (13) and (14) could be written with Eq. (14) as follows:

$$\frac{d\varepsilon_r}{dt}=-\frac{V_r}{L_{rb}}-\left(-\frac{dI_r^{ref}}{dt}+V_r^{dis}\right) \tag{15}$$

Next, the desired closed-loop dynamics can be written as:

$$\frac{d\varepsilon_r}{dt}+K\varepsilon_r=0, \tag{16}$$

where $K=\begin{bmatrix} k_d & k_q \end{bmatrix}$ is defined as proportional controller gain.

If Eq. (15) is written into Eq. (16), the desired closed-loop dynamics are rewritten as follows:

$$-\frac{V_r}{L_{rb}}+(\frac{dI_r^{ref}}{dt}+V_r^{dis})-K\varepsilon_r=0. \tag{17}$$

The rotor voltage equations could be obtained by rewriting Eq. (17):

$$V_r^{ref}=L_{rb}(\frac{dI_r^{ref}}{dt}+V_r^{dis}+K\varepsilon_r). \tag{18}$$

If the effect of $\frac{dI_r^{ref}}{dt}$ is neglected, the control effort could be expressed as follows:

$$V_r^{ref}=V_r^{dis}+L_{rb}K\varepsilon_r. \tag{19}$$

### 3.3. Disturbance observer

In this section, the derivation of the disturbance observer is presented. The vector $V_r^{dis}$ is the disturbance term, which is dependent on physical conditions. The controller structure can be finalized if the disturbances are correctly estimated:

$$V_r^{dis}=V_r-L_{rb}\frac{dI_r}{dt}. \tag{20}$$

Writing Eq. (20) in the s domain and implementing the first-order low-pass filter disturbance observer concept [17]:

$$\hat{V}_r^{dis}=(V_r-L_{rb}\frac{dI_r}{dt})\frac{g}{s+g}. \tag{21}$$

The estimation error can be expressed as:

$$V_r^{dis}-\hat{V}_r^{dis}=(V_r-L_{rb}\frac{dI_r}{dt})-(V_r-L_{rb}\frac{dI_r}{dt})\frac{g}{s+g}=(1-\frac{g}{s+g})V_r^{dis}. \tag{22}$$

The estimation error converges to zero. Vector $\hat{V}_r^{dis}=\begin{bmatrix} \hat{v}_{rd}^{dis} & \hat{v}_{rq}^{dis} \end{bmatrix}$ is the parameter-dependent estimated disturbance. The term g is the cut-off frequency of the low-pass filter in radians. It is obvious from Eq. (21) that $\hat{v}_{rd}^{dis}$ and $\hat{v}_{rq}^{dis}$ are independent of machine parameters. As a result, the block diagram in Figure 3 could be obtained. Decoupled control of active and reactive power could be achieved by controlling $i_{rq}$ and $i_{rd}$, respectively. This control structure can be implemented in speed, torque, or power control of DFIG. Maximum power point tracking algorithms can be followed according to any wind turbine dynamics.

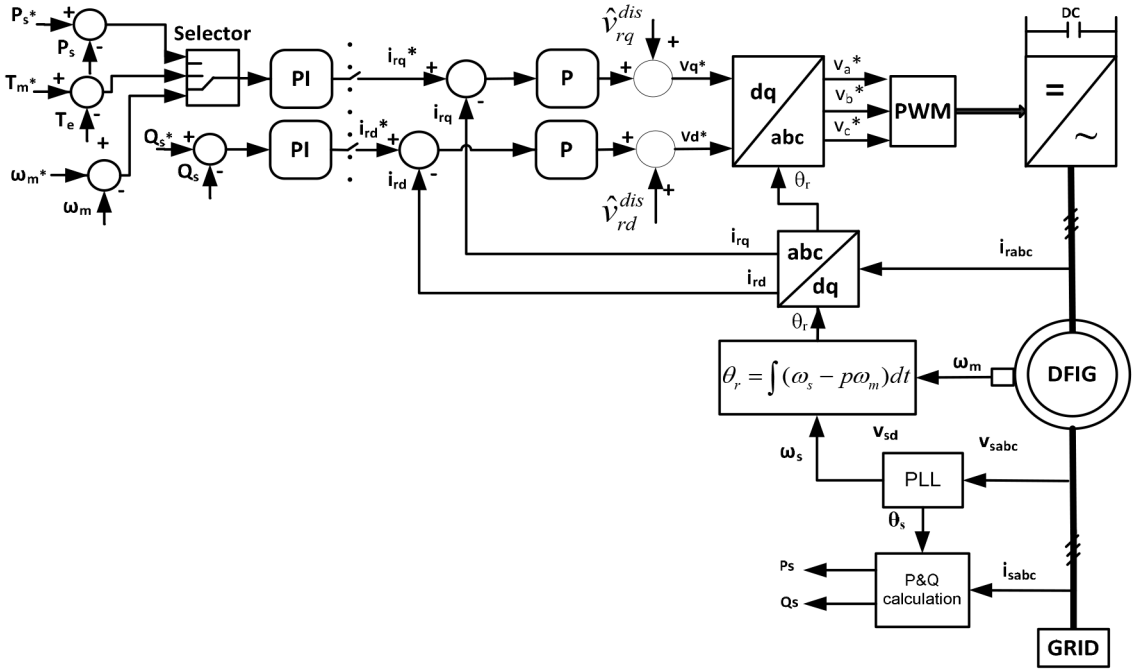


**Figure 3**. Proposed control diagram.

### 3.4. Simulation results

A more accurate simulation platform is obtained as compared with [3] without the necessity of reduced-order models by using a discretized model of DFIG. A 100-$\mu$s sample time in MATLAB/Simulink is used in simulations. Inverter dynamics are neglected. The 500 kW DFIG parameters [18] that will be used in the MİLRES project are given in Table 1. All rotor parameters are referred to the stator side. The control system can work in different scenarios. In the current study, the generator is controlled according to the speed control strategy.

**Table 1.** DFIG parameters in simulation.

| | | |
|---|---|---|
| Stator power ($P_s$) | 457.6 | kW |
| Rotor power ($P_r$) | 61.4 | kW |
| Stator voltage | 690 | V |
| Number of poles (p) | 4 | |
| Slip variation | 0.25 | |
| Nominal torque | 6784 | Nm |
| Synchronous speed | 750 | rpm |
| Stator resistance ($R_s$) | 0.018 | ohm |
| Rotor resistance ($R_r$) | 0.021 | ohm |
| Mutual inductance ($L_m$) | 0.011 | H |
| Stator inductance ($L_s$) | 0.012 | H |
| Rotor inductance ($L_r$) | 0.012 | H |
| Turn ratio ($n_s/n_r$) | 4 | |
| Moment of inertia | 22 | $kgm^2$ |

Machine parameter-dependent compensating terms of the control structure are estimated by a disturbance observer. Basically, two different step-response tests are applied in one simulation at different time instants. Speed reference is changed from 60 to 90 rad/s (from subsynchronous to supersynchronous speeds) at the 10th second. Wind torque reference is changed from 3000 Nm to 5000 Nm at the 12th second. It is expected that the system must follow the speed (Figure 4) and wind torque (Figure 5) while accurately estimating the disturbance terms. There is a huge current torque and current increase at the 10th second of simulation. The reason for the high current and torque is the speed step, which is deliberately applied with a high speed controller gain in order to check the performance of the controller structure. The control system could handle this dramatic step and remained stable. The $i_{rd}$ reference (Figure 6) was kept at zero during the simulations.

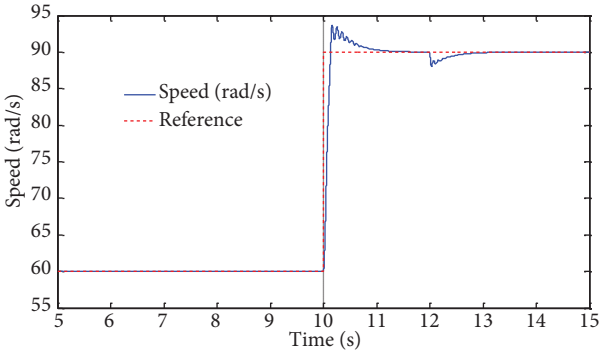


**Figure 4.** Actual and reference speed.

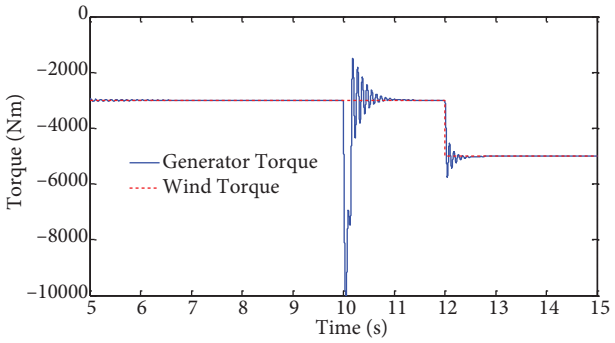


**Figure 5.** Generator torque and wind torque.

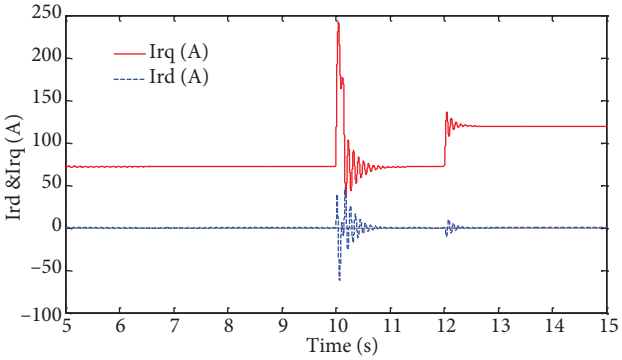


**Figure 6.** Rotor currents.

Active and reactive stator powers are decoupled (Figure 7). Rotor power changes the direction while the speed changes from subsynchronous to supersynchronous (Figure 8). It is obvious from the simulation results that the DFIG dynamic model works properly and the compensating terms are accurately estimated by the disturbance observer (Figures 9 and 10). The performance of the speed controller could be modified (Figure 4) according to physical conditions. However, the focus of the simulation results is the accurate estimation of compensating terms.

## 4. Experimental results

The experimental setup in Figure 11 was used in the experiments and results are shown in Figures 12–21. A squirrel-cage induction machine (SCIM) was driven by a commercial inverter that represents the wind.

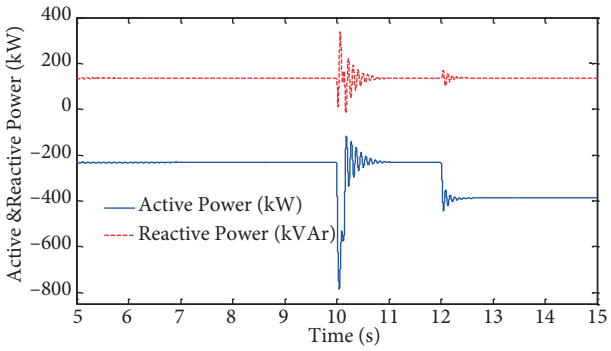


**Figure 7.** Stator active and reactive power.

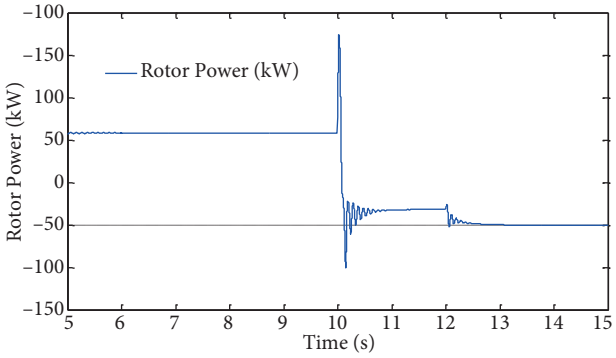


**Figure 8.** Rotor active power.

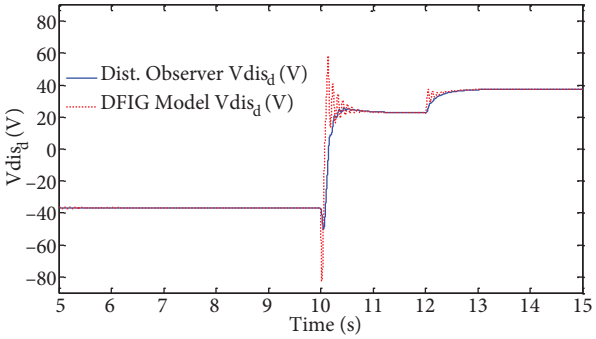


**Figure 9.** Estimated and modeled disturbance terms ($v_{disd}$).

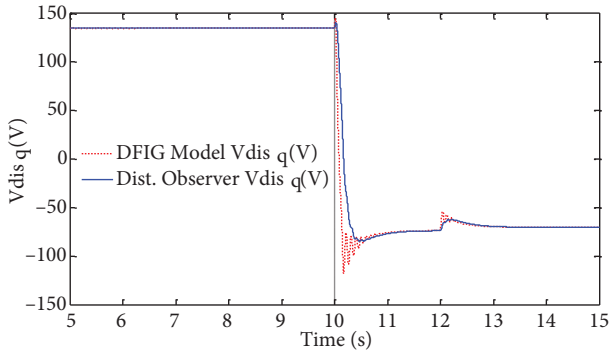


**Figure 10.** Estimated and modeled disturbance terms ($v_{disq}$).

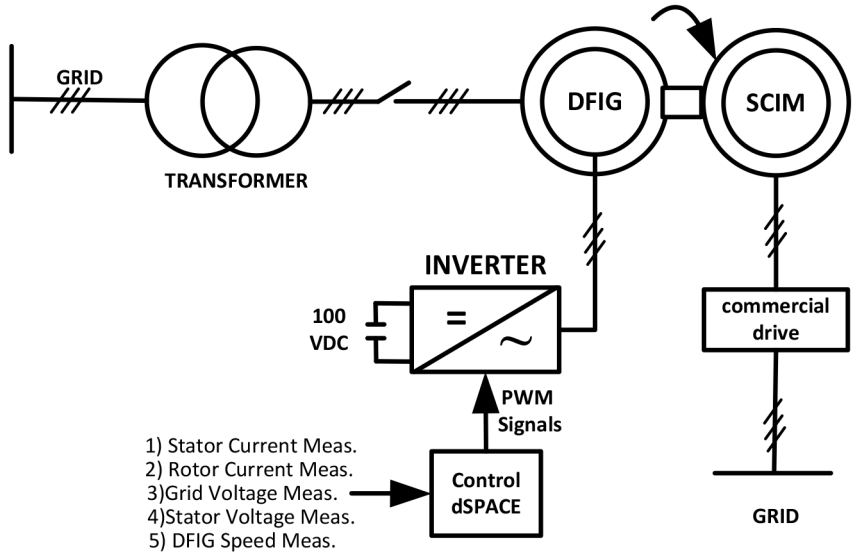


**Figure 11.** Experimental setup.

The DFIG plate data are given in Table 2. The controller algorithm is generated in dSPACE DS1103 by using Controldesk C language. The sample time of the control structure is 100 $\mu$s. A Semikron Semistack (21f_b6u_e1cif_b6ci_12_v12) inverter used in the experiments and 120 V DC constant voltage power is directly applied to the DC link. The switching frequency is 10 kHz. The low-pass filter cut-off frequency (g) is chosen as 1200. The proportional gains of the controllers ($k_p$ and $k_q$) are 100. These values were found by trial and error during the experiments without any algebraic calculations.

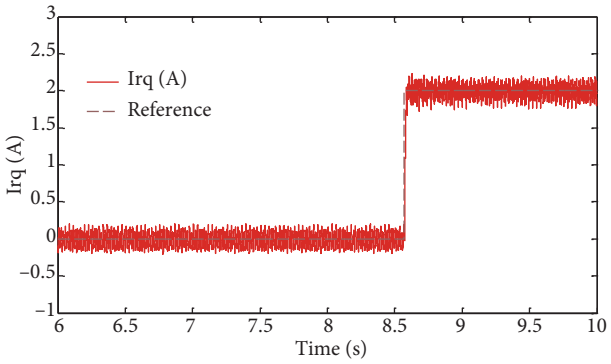


**Figure 12.** Experiment 1-A, $I_{rq}$ step response.

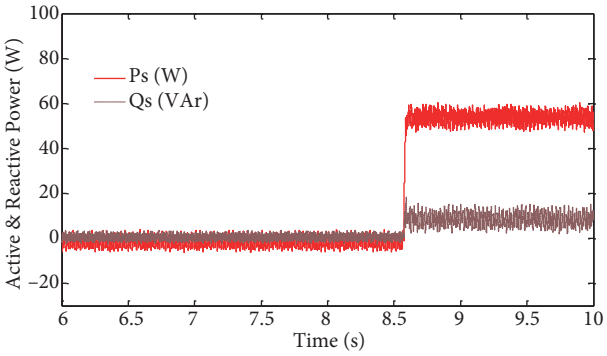


**Figure 13.** Experiment 1-A, change of active and reactive power.

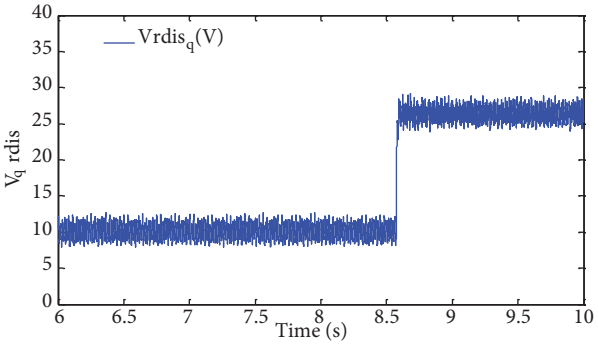


**Figure 14.** Experiment 1-A, compensating term Sq.

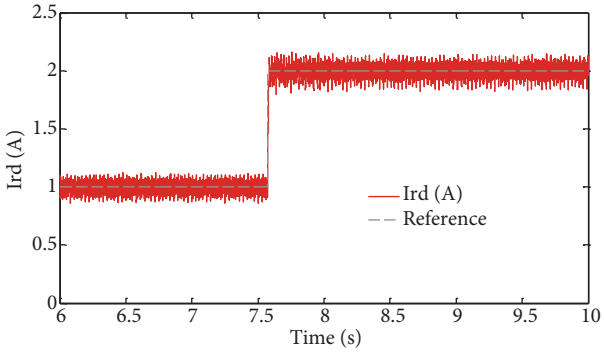


**Figure 15.** Experiment 1-B, $I_{rd}$ step response.

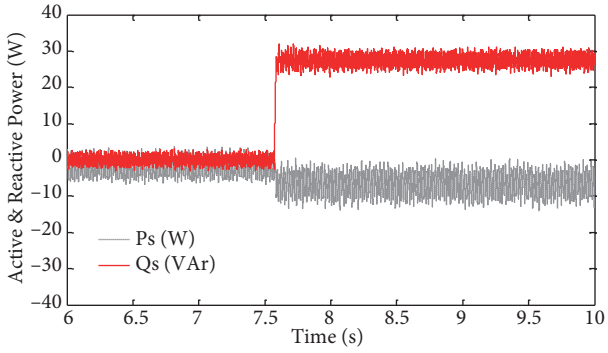


**Figure 16.** Experiment 1-B, change of active and reactive power.

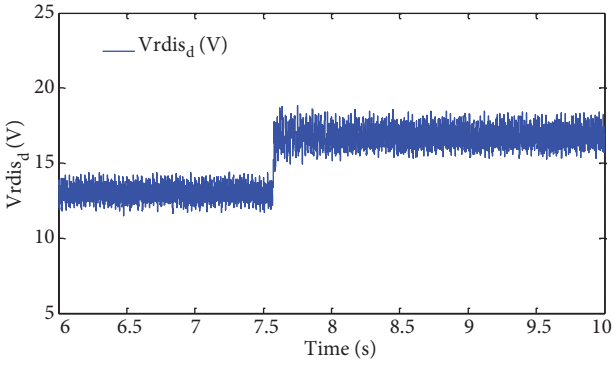


**Figure 17.** Experiment 1-B, Vrdis_d.

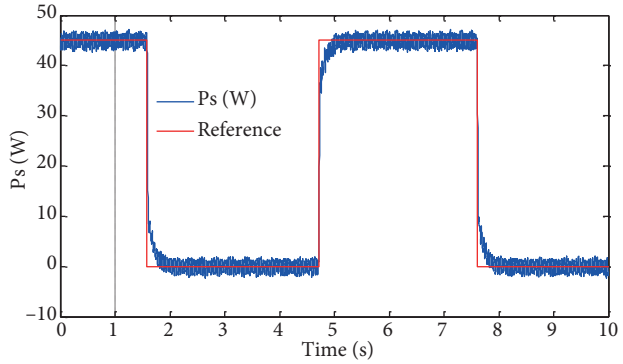


**Figure 18.** Experiment 2-A, active power response test.

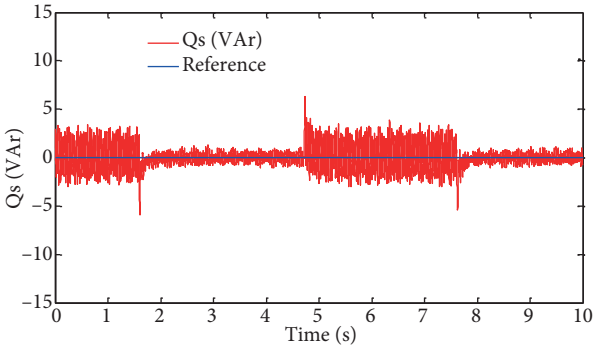


**Figure 19.** Experiment 2-A, reactive power at active power step response test.

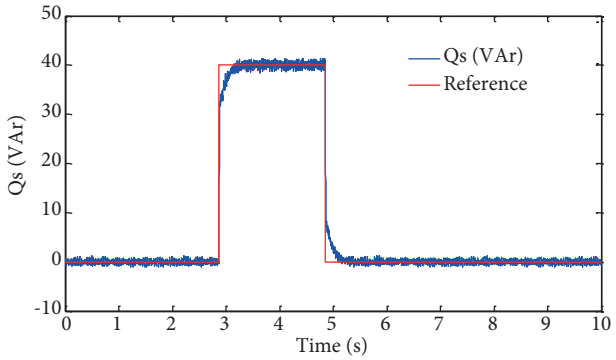


**Figure 20.** Experiment 2-B, reactive power response test.

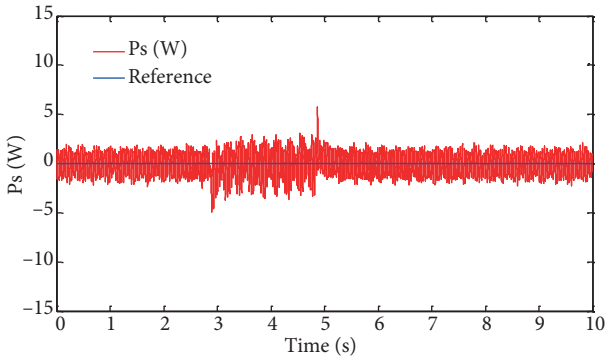


**Figure 21.** Experiment 2-B, active power at reactive power response test.

**Table 2.** DFIG plate data in experiments.

| | | |
|---|---|---|
| Power | 1.1 | kW |
| Stator voltage | 220/380 | V (D/Y) |
| Stator current | 6.4/3.7 | A |
| Power factor | 0.67 | |
| Speed | 1360 | rpm |
| Rotor voltage | 70 | V |
| Rotor current | 12 | A |

### 4.1. Experiment 1

The aim of the first experiment is to show that decoupled control of $I_{rd}$ and $I_{rq}$ rotor currents separately changes the stator active and reactive power, respectively. The DFIG is rotated in constant subsynchronous speed by the SCIM. $I_{rd}$ and $i_{rq}$ step-response tests are applied in different experiments, and the change of the stator reactive and active power is respectively demonstrated.

It is obvious from the experimental results that both rotor current controllers accurately change stator active and reactive power (Figures 13 and 16). Compensating terms also change (Figures 14 and 17) when step responses are applied.

### 4.2. Experiment 2

The main objective of DFIG-based wind turbines is decoupled control of active and reactive power. The control structure given in Figure 3 is implemented by using basic PI power controllers in the outer loop while the generator is driven by the SCIM at an arbitrary speed. Active and reactive power step response tests are applied and decoupled control of active and reactive stator power can be achieved.

## 5. Conclusion

Decoupled control of active and reactive power with a first-order low-pass filter disturbance observer is fully demonstrated with the simulation and experimental results. It is shown that compensating terms are accurately estimated by the disturbance observer in simulations. The experimental results validate the accuracy of the proposed control method by effectively achieving stator active and reactive power flow.

**Symbol nomenclature**

| | |
|---|---|
| $i_{sa}, i_{sb}, i_{sc}$ | Stator a, b, and c phase currents |
| $i_{sd}, i_{sq}$ | Stator d and q axis currents |
| $i_{ra}, i_{rb}, i_{rc}$ | Rotor a, b, and c phase currents |
| $i_{rd}, i_{rq}$ | Rotor d and q axis currents |
| $v_{sa}, v_{sb}, v_{sc}$ | Stator a, b, and c phase voltages |
| $v_{s\alpha}, v_{s\beta}$ | $\alpha$ and $\beta$ axis stator voltage |
| $v_{ra}, v_{rb}, v_{rc}$ | Rotor a, b, and c phase voltages |
| $v_{sd}, v_{sq}$ | Stator d and q axis voltages |
| $v_{rd}, v_{rq}$ | Rotor d and q axis voltages |
| $R_s, R_r$ | Stator and rotor resistances |
| $P_s,$ | Stator active power |
| $Q_s$ | Stator reactive power |
| $L_s, L_r$ | Stator and rotor inductances |
| $L_m$ | Mutual inductance |
| $L_{rb}$ | Base value of rotor inductance |
| $\Delta L_r$ | Disturbance of $L_r$ |
| $p$ | Number of pole pairs |
| $\omega_s$ | Stator electrical speed |
| $\omega_m$ | Rotor mechanical speed |
| $T_m$ | Mechanical torque |
| $T_e$ | Electrical torque |
| $b$ | Viscous friction constant |
| $\theta_s$ | Stator electrical angle |
| $\theta_r$ | Rotor electrical angle |
| $T_s$ | Sample time |
| $s$ | Laplace operator |
| $k_p, k_q$ | Proportional gain of controller |

## References


[1] Montenau I, Bratcu AI, Cutululis NA, Ceanga E. Optimal Control of Wind Energy Systems: Towards a Global Approach. Advances in Industrial Control. London, UK: Springer, 2008.

[2] Leonhard W. Control of Electrical Drives. 3rd ed. Berlin, Germany: Springer, 2001.

[3] Akhmatov V. Analysis of dynamic behavior of electric power systems with large amount of wind power. PhD thesis, Technical University of Denmark, Kongens Lyngby, Denmark, 2003.

[4] Pena R, Clare JC, Asher GM. A doubly-fed induction generator using two back-to-back PWM converters and its application to variable speed wind energy system. P IEE 1996; 143: 231–241.

[5] Muller S, Deicke M, De Doncker RW. Doubly fed induction generator systems for wind turbines. IEEE Ind Appl Mag 2002; 8: 26–33.

[6] Li S, Challoo R, Nemmers MJ. Comparative study of DFIG power control using stator-voltage and stator-flux oriented frames. In: Power & Energy Society General Meeting, 2009; Calgary, Canada. New York, NY, USA: IEEE, pp. 1–8.

[7] Demirok E. Grid-connected variable speed generator applications with doubly-fed induction machine. MSc, Sabancı University, İstanbul, Turkey, 2007.

[8] Tapia G, Santamaria G, Telleria M, Susperregui A. Methodology for smooth connection of doubly fed induction generators to the grid. IEEE T Energy Conver 2009; 24: 959–971.

[9] Xu L, Cartwright, P. Direct active and reactive power control of DFIG for wind energy generation. IEEE T Energy Conver 2006; 3: 750–758.

[10] Zhi D, Xu L. Direct power control of DFIG with constant switching frequency and improved transient performance. IEEE T Energy Conver 2007; 22: 110–118.

[11] Battista HD, Mantz RJ. Dynamical variable structure controller for power regulation of wind energy conversion systems. IEEE T Energy Conver 2004; 4: 756–763.

[12] Beltran B, BenBouzid MEH, Ahmet-Ali T. High order sliding mode control of a DFIG based wind turbine for power maximization and grid fault tolerance. In: Electric Machines and Drives Conference (IEMDC), 2009; Miami, FL, USA. New York, NY, USA: IEEE, pp. 183–189.

[13] Luna A, Rolan A, Medeiros G, Rodrigez P, Teodorescu R. Control strategies for DFIG wind Turbines Under Grid Fault Conditions. In: 35th Annual Conference of IEEE Industrial Electronics (IECON), 2009; Porto, Portugal. New York, NY, USA: IEEE, pp. 3886–3891.

[14] Rodriguez P, Luna A, Teodorescu R, Iov F, Blaabjerg F. Fault ride-through capability implementation in wind turbine converters using a decoupled double synchronous reference frame PLL. In: European Conference on Power Electronics, 2007; Aalborg, Denmark. New York, NY, USA: IEEE, pp. 1–10.

[15] Zhou P, Yikang H, Sun D. Improved direct power control of a DFIG-based wind turbine during network unbalance. IEEE T Power Electr 2009; 11: 2465–2474.

[16] Blaabjerg F, Teodorescu R, Liserre M, Timbus AV. Overview of control and grid synchronization for distributed power generation systems. IEEE T Ind Electron 2006; 5: 1398–1409.

[17] Ohnishi K, Shibata M, Murakami T. Motion control for advanced mechatronics. IEEE-ASME T Mech 1996; 1: 56–67.

[18] TÜBİTAK Report. Generatör Elektriksel ve Manyetik Analiz Detay Tasarım Raporu (DFIG), R-1.1.1. Ankara, Turkey: TÜBİTAK, 2013 (in Turkish).